# Evolution of nontrivial Fermi surface features in the band structures of the homologous members $Pb_5Bi_6Se_{14}$ and $Pb_5Bi_{12}Se_{23}$

D. Koumoulis,[1,*] L. Fang,[2] D. Y. Chung,[3] M. G. Kanatzidis,[2,3,†] and L.-S. Bouchard[1,4,‡]
[1] *Department of Chemistry and Biochemistry, University of California, Los Angeles, California 90095-1569, USA*
[2] *Department of Chemistry, Northwestern University, Evanston, Illinois 60208, USA*
[3] *Division of Materials Sciences, Argonne National Laboratory US DOE, Argonne, Illinois 60439, USA*
[4] *California NanoSystems Institute, UCLA, Los Angeles, California 90095, USA*

(Received 18 January 2020; revised manuscript received 9 March 2020; accepted 11 March 2020; published 30 March 2020)

High-quality single crystals of $(PbSe)_5(Bi_2Se_3)_{3m}$ were grown and analyzed by nuclear magnetic resonance (NMR) spectroscopy. We report on $^{77}Se$ and $^{207}Pb$ NMR shifts and nuclear spin-lattice relaxation measurements in the naturally formed heterostructure homology $(PbSe)_5(Bi_2Se_3)_{3m}$ with $m = 1$ ($Pb_5Bi_6Se_{14}$) and $m = 2$ ($Pb_5Bi_{12}Se_{23}$). A distinct site-specific contribution has been detected for both nuclei as a function of temperature, which reveals an electronic changeover from a semiconducting $Pb_5Bi_6Se_{14}$ to a semimetalliclike $Pb_5Bi_{12}Se_{23}$ system with nontrivial band structure features near the Fermi level. The temperature dependences of the relaxation rates are dominated by significant changes in the topology of energy dispersions accompanied with band edges and crossings in the region of the Fermi surface. These results, which interrogate nuclear spin interactions from selected atomic sites, clearly expose the effects of the added $Bi_2Se_3$ layer on the crystal and electronic structure of $Pb_5Bi_{12}Se_{23}$. These findings provide direct microscopic insight into the unconventional and dual nature of the electronic structure of these homologous thermoelectric and topologically nontrivial compounds.

DOI: 10.1103/PhysRevB.101.115309

## I. INTRODUCTION

The design and synthesis of advanced topological insulating materials for novel efficient thermoelectric [1] and optoelectronic properties [2] is currently of high interest in solid-state chemistry and materials engineering. It requires the design of low-cost and highly efficient materials that can enable conversion (via a solid-state process) of heat into electricity by showing enhanced carrier mobility accompanied with low lattice thermal conductivity, as well as exhibit optical properties such as field-effect transistors (FETs) [2]. In this work, a naturally formed heterostructured material comprises alternating layers of PbSe and $Bi_2Se_3$, as expressed by the homologous formula $(PbSe)_5(Bi_2Se_3)_{3m}$, where $m = 1, 2$ [1,3] has been studied. This homologous series combines two prototype materials: PbSe, a well-studied thermoelectric (TE) and $Bi_2Se_3$, a prototypical topological insulator (TI) material. As a result, a multifunctional material with dual properties is expected. The value of $m$ designates the number of $Bi_2Se_3$ sheets that are sandwiched by consecutive PbSe slabs. The $Bi_2Se_3$ sheet is hexagonal and is identical to a quintuple layer (QL) of the topological insulator $Bi_2Se_3$. The PbSe sheet has tetragonal symmetry and is a two-atom-thick slice from the face-centered-cubic (FCC) structured PbSe. The lattice mismatch between $Bi_2Se_3$ and PbSe produces a stress that strongly distorts the slab of PbSe along the $c$ axis for both homologous phases. Regarding the band structure characteristics of this series, Nakayama *et al.* [4] provided experimental evidence for the existence of a dramatic change in the electronic states' character around the Fermi energy related to an upgraded band inversion (BI) process associated with a three-dimensional (3D) to two-dimensional (2D) crossover due to the layering symmetry of the $(PbSe)_5(Bi_2Se_3)_{3m}$ series [4]. Band inversion plays a key role in the alteration of the topological order [4,5] through a band splitting originating mainly by the strong spin-orbit coupling as well as lattice distortions and defects [4–6]. As originally proposed by Dimmock *et al.* [7], during the BI process a band-gap evolution takes place upon doping through a systematic closing and gradual reopening of the gap between the conduction and valence bands. As a result, there is an inverted band symmetry related to the former (e.g. $Pb_xSn_{1-x}Te$ [6,7], $(PbSe)_5(Bi_2Se_3)_{3m}$ [4,8] etc.). Scalar relativistic, electronic, and structural terms are essential contributions to the BI mechanism. Furthermore, the $m = 1$ phase features a large number of chemical bonds with a length of ~3.25 Å between the PbSe and $Bi_2Se_3$ sheets, creating a 3D structure. In the $m = 2$ phase, the two adjacent QLs II and III are connected by van der Waals bonding. This weak bonding relaxes the stress and preserves the uniformity of the $Bi_2Se_3$ sheets. Crystal cleaving always occurs along the van der Waals plane and exposes an ideal surface of $Bi_2Se_3$ with Dirac fermions residing on it. By contrast, crystal cleavage in the $m = 1$ phase breaks the chemical bonding between PbSe

---

[*] dimkoum@chem.ucla.edu
[†] m-kanatzidis@northwestern.edu
[‡] bouchard@chem.ucla.edu

and $Bi_2Se_3$, likely leaving a large number of dangling bonds on top of the $Bi_2Se_3$ slab.

An angle-resolved photoemission spectroscopy (ARPES) study on $m = 1$ and $m = 2$ phases by Nakayama *et al.* [4]. and first-principles calculations by Momida *et al.* [8] have shown a marked difference in the band dispersions near the Fermi level ($E_F$) in these two samples. Namely, the band structure for $m = 1$ is a single parabolic band, whereas for $m = 2$ the band structure consists of multiple bands associated with a shallow dip at the top due to the presence of additional bands that cross $E_F$. The $m = 2$ sample has a more complicated band structure than $m = 1$. The presence of a large gap of approximately 0.5 eV in the topological states as well as the even number of $E_F$ crossings of the bands indicate that the $m = 2$ sample cannot be classified within the framework of known topological insulating materials. In particular, ARPES experiments on $m = 2$ [4] revealed six dispersive features around the near-$E_F$ region where two of them cross $E_F$ and overlap with the Dirac-cone surface states, which mainly originate from the $Bi_2Se_3$ layers. Recent *ab initio* calculations [8] for the $m = 2$ system have shown that its electronic structure near the Fermi energy consists of a mixture of $Bi_2Se_3$- and PbSe-layer bands.

Herein we report results of a combined $^{77}$Se and $^{207}$Pb NMR investigation carried out on $Pb_5Bi_6Se_{14}$ ($m = 1$) and $Pb_5Bi_{12}Se_{23}$ ($m = 2$) to explore at the microscopic level the unusual electronic features that have been predicted from band structure calculations performed on $(PbSe)_5(Bi_2Se_3)_{3m}$. During the BI process that arises from a continuous transition from $m = 1$ to $m = 2$, $^{207}$Pb and $^{77}$Se NMR spectra as well as nuclear spin-lattice relaxation rates (variable temperature) provide electronic characterization of the electronic energy bands that cross or lie near the Fermi level [6,9–11], and provide a better understanding of the topologically nontrivial features of the Fermi-level density of states for $(PbSe)_5(Bi_2Se_3)_{3m}$.

## II. EXPERIMENTAL DETAILS

A ground powder mixture (total 5 g scale) of PbSe and $Bi_2Se_3$ with a stoichiometric ratio for $m = 1$ and $m = 2$ was loaded in a silica-fused tube (12 mm OD) and sealed under vacuum at $10^{-4}$ mbar. The mixture was melted at 750 °C for 1 h, followed by slow cooling at 2 °C/h to room temperature. The respective synthesis for $m = 1$ and $m = 2$ produced single crystal whiskers and an ingot. Thermopower measurements were performed on the polycrystalline pellet samples. The pellet samples were prepared by sintering a stoichiometric mixture of fine powder of PbSe and $Bi_2Se_3$ to prevent the formation of second phases that can form above the melting points (744 °C for $m = 1$ and 690 °C for $m = 2$) of the compounds by peritectic decomposition. The synthesis was processed at 600 °C and 550 °C for $m = 1$ and $m = 2$, respectively, for 10 days and produced agglomerates of the target compound at a quantitative yield of nearly pure phase. The sample for thermopower was prepared by cold press and annealing at 500 °C for 3 days. The measured density of the pellet samples was about 97% of the calculated value. We confirmed that the anisotropic effect of thermopower on these compounds is very small at room temperature [12]. The carrier density of our samples was not measured and cannot be evaluated directly from that of the Sassi *et al.* [13] compound with $m = 2$ because of different doping levels of the samples prepared in different conditions. However, we speculate that the carrier density is of the same order of magnitude as their thermopowers are, in a narrow range from $-50$ to $-30$ $\mu$V/K. Also, the carrier density of the compound $m = 1$ may be lower than that of the $m = 2$ compound based on the thermopower data on the samples prepared under the same conditions. More details about the synthesis procedure and characterization of the homologous $(PbSe)_5(Bi_2Se_3)_{3m}$ series can be found in Refs. [1,3]. The NMR measurements were performed on a Bruker DSX-300 spectrometer operating at a frequency of 62.79 MHz for lead ($^{207}$Pb) and 57.24 MHz for selenium ($^{77}$Se) nuclei [14–16]. The chemical shift scales were calibrated using the $\Xi$ scale [12], where the reference compounds for defining 0 ppm on the chemical shift scales were the tetramethyllead ($^{207}$Pb) and dimethylselenide ($^{77}$Se) [14]. Static polycrystalline samples of $Pb_5Bi_6Se_{14}$ ($m = 1$) and $Pb_5Bi_{12}Se_{23}$ ($m = 2$) were placed in a 5-mm solenoid coil of a standard Bruker X-nucleus NMR probe. All samples were ground with a mortar and pestle to reduce radiofrequency (rf) skin-depth effects at these NMR frequencies. The $^{207}$Pb $\pi/2$ pulse width was 4.5 $\mu$s. The $^{77}$Se $\pi/2$ pulse width was 4.0 $\mu$s. Spectral (lineshape) data were acquired using a spin-echo sequence $[(\pi/2)_x\text{–}\tau\text{–}(\pi)_y\text{–}\tau\text{-acquire}]$ with the echo delay, $\tau$, set to 20 $\mu$s. Nuclear spin-lattice relaxation times ($T_1$) were measured with a saturation recovery technique for both $^{77}$Se and $^{207}$Pb nuclei for all samples [15,16].

## III. RESULTS AND DISCUSSION

Numerous studies have shown that NMR static and dynamic parameters can probe the coupling of specific lattice site nuclei to the electronic band charge carriers, as well as to the quadrupolar effects [6,9,15–35]. This is a (selective) site-specific benefit of NMR spectroscopy compared to other techniques, which can be used to probe the involvement of local orbitals and hybridization effects in the conduction process. Since 2012 [21,31] there have been many demonstrations via NMR experiments and theoretical analyses [25,27] of the usefulness of the NMR frequency shift at probing strong relativistic effects as well as unusual electronic characteristics and band features of TI and TE materials. The aforementioned sensitivity to relativistic effects (e.g., spin-orbit coupling) due to the presence of heavy $Z$ elements in alloys is an essential parameter for manifestation of the BI effect. The BI depends on the nature of the charge carrier, charge carrier and/or lattice defect density (as well as impurities), and electronic inhomogeneities [15,21,30,31,35]. All the aforementioned parameters can be detected via the nuclear spin-lattice relaxation mechanism and Knight shift [9,16,19], using sensitive atomic-level probes that can accurately assess the *s*- or non-*s* electron nature at the density of states at the Fermi level [9,35–40].

Figure 1 presents the static $^{77}$Se NMR spectra of two powdered samples $(PbSe)_5(Bi_2Se_3)_{3m}$, $m = 1, 2$ at ambient temperature (296 K). For both samples, a single resonance was observed. Both spectra are well described by a Gaussian lineshape. The $m = 1$ sample shows the $^{77}$Se resonance at $-98.05$ ppm, while for $m = 2$ it lies at $-16.69$ ppm. A detailed study via $^{77}$Se NMR on PbSe and $Bi_2Se_3$ can

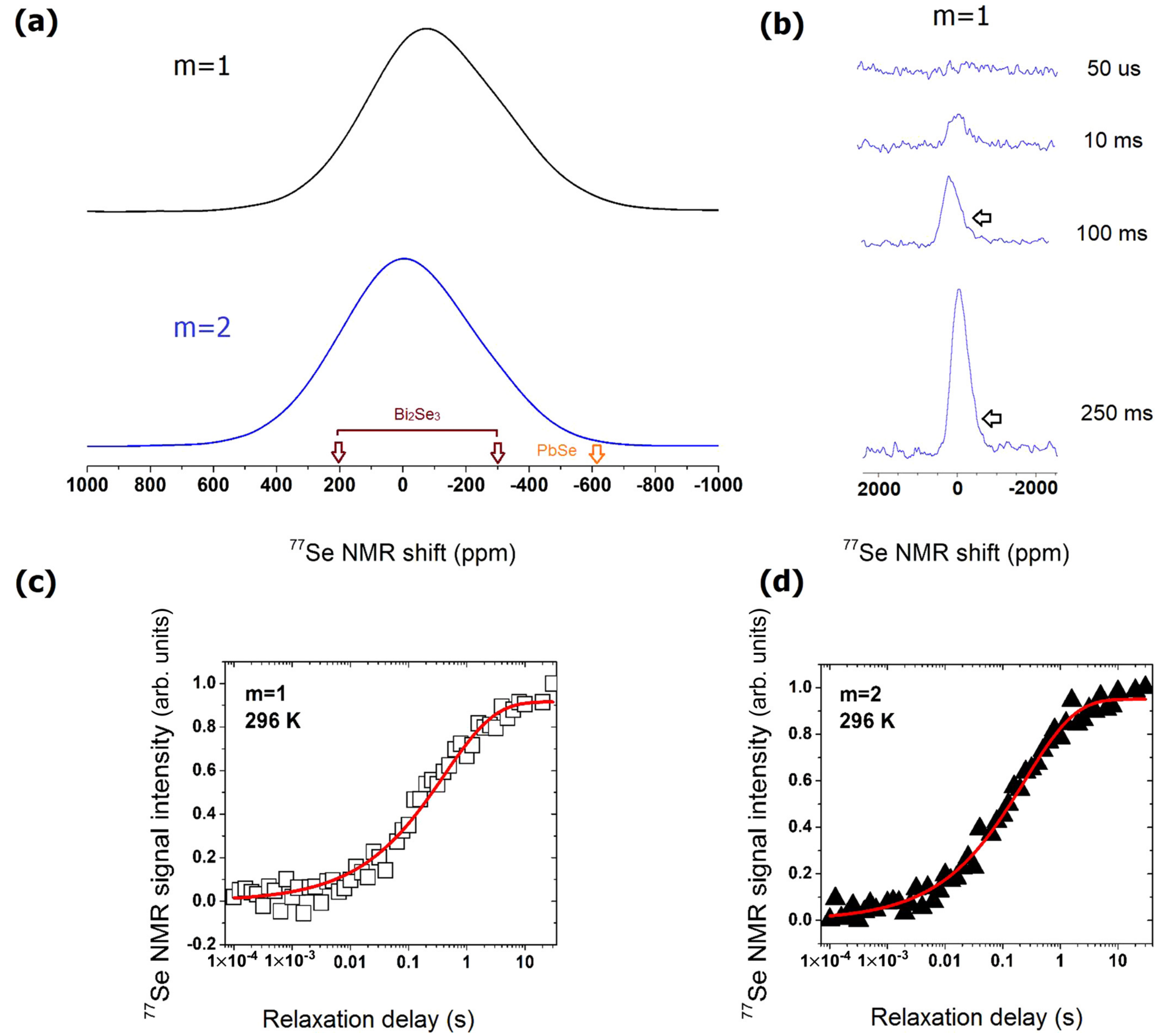

FIG. 1. (a) Static $^{77}$Se NMR spectra measurements of (PbSe)$_5$(Bi$_2$Se$_3$)$_{3m}$ for $m = 1$ and $m = 2$, at 7.05 T and at ambient temperature. The positions of the different Se sites are shown on the frequency scale (ppm) for both Bi$_2$Se$_3$ and PbSe, as has been reported in Refs. [31,15]. (b) The $^{77}$Se spectrum for $m = 1$ when acquired during the saturation recovery relaxation experiments at different delays (50 $\mu$s–250 ms). $^{77}$Se magnetization recovery curves of (PbSe)$_5$(Bi$_2$Se$_3$)$_{3m}$ for $m = 1$ (c) and $m = 2$ (d) at 296 K. The solid red line represents a stretched exponential fit.

be found in Ref. [15] and Refs. [31–33,41], respectively. Recently, comprehensive $^{77}$Se NMR studies on single crystals of Bi$_2$Se$_3$ revealed the presence of nonequivalent crystallographic Se sites in the spectra with the crystallographic *c* axis parallel and perpendicular to the external magnetic field [32,33,41]. When dealing with powders, such sites overlap and are difficult to resolve.

For $m = 1$ and $m = 2$, negative values of the resonance shift are expressed as $K^{77} = K_s^{77} + K_{\mathrm{orb}}^{77}$, where $K_s^{77}$ represents the Knight shift associated with the *s*-contact term, and $K_{\mathrm{orb}}^{77}$ is the temperature-independent shift originating from orbital electrons. The Fermi-contact term reflects the magnetic coupling of the $^{77}$Se nucleus to the *s* character of conduction electrons [15,37], written as $K^{77} = \frac{16\pi}{3}\mu_{\mathrm{B}}^2\langle|\psi(0)|^2\rangle_{\mathrm{E}_F}N(E_F)$, where $\mu_B^2$ is the Bohr magneton squared, the $\langle|\psi(0)|^2\rangle_{E_F}$ term is the average probability density at the nucleus for electronic states around the Fermi level ($E_F$), and $N(E_F)$ is the density of states (DOS) at $E_F$ [36,37,42]. Both samples here are *n*-type semiconductors; hence the sign of the resonance shift is the same for both. However, the $m = 1$ sample has a smaller downfield shift than the $m = 2$ sample, which means that the carrier density is reduced in this compound relative to the $m = 2$ case. To shed light on this divergence, we measured the Seebeck coefficients of these compounds. The $m = 1$ sample had a room-temperature Seebeck coefficient value equal to $-131$ $\mu$V/K, whereas the value for $m = 2$ was $-52$ $\mu$V/K. Thus, both samples are *n*-type semiconductors. Similarly, measurements of the carrier density of both $m = 1$

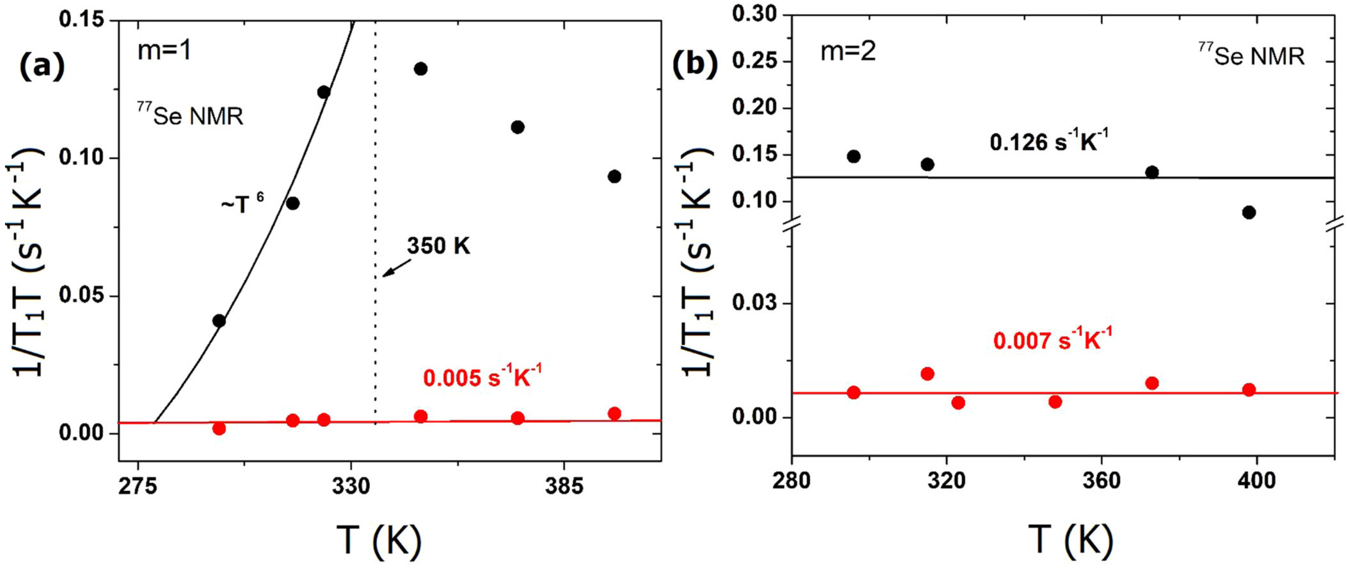

FIG. 2. $^{77}$Se nuclear spin-lattice relaxation contributions as a function of temperature for $m = 1(\mathrm{Pb_5Bi_6Se_{14}})$ and $m = 2(\mathrm{Pb_5Bi_{12}Se_{23}})$, as shown in (a,b), respectively. The $1/T_1T$ values were derived by using the double exponential function, as explained in the text. The suppression in the DOS at the Fermi energy (gap opening) is evident in the $m = 1$ case (a), as seen by an abrupt decrease of $1/T_1T$ whereas in the case of $m = 2$ a temperature-independent Korringa process holds (typical of gapless behavior) for both relaxation components (b).

and $m = 2$ performed by Sassi *et al.* [13] have demonstrated the *n*-type heavily doped nature of these materials.

Combining the semiclassical Mott-Jones formula, according to which the Seebeck coefficient is inversely proportional to the carrier density ($S \sim n^{-\frac{2}{3}}$), with the sign and magnitude of the $^{77}$Se Knight shift, which is governed by the Fermi-contact term and directly proportional to the density of states (DOS) at the Fermi level ($E_F$), we conclude that the large $^{77}$Se NMR shift reflects the strong coupling between the spin of charge carriers to the magnetic moment of $^{77}$Se nuclei via hyperfine interactions. Furthermore, the enhanced $^{77}$Se NMR downfield shift of $m = 2$ compared to $m = 1$ derives mainly from a larger amount of *s*-character electrons at the Fermi surface of $m = 2$ compared to $m = 1$.

Lastly, as shown in Fig. 1, the linewidth calculated as full width at half maximum (FWHM) was found to be $\mathrm{FWHM}^{77}_{m=1} = 512$ ppm ($\sim$29 kHz) for $m = 1$ and $\mathrm{FWHM}^{77}_{m=2} = 516.89$ ppm ($\sim$30 kHz) for $m = 2$. According to the crystallography of these materials [3,4,13,43], a misfit exists between the PbSe and $\mathrm{Bi_2Se_3}$ layers that promotes lattice distortions and gives rise to a distorted octahedral structure, especially near the boundaries. The large carrier density that appears in the $m = 2$ sample derives mainly from the doping of Se vacancy, analogous to that of $\mathrm{Bi_2Se_3}$ [3] as well as the presence of antisite defects (Pb/Bi) could also explain the difference or a higher concentration of positively charged defects in the $m = 1$ compound.

In view of the fact that selenium has a nuclear spin of $I = 1/2$ and zero nuclear quadrupole moment, the presence of native defects and the aforementioned lattice distortions should not affect the correlation between linewidth behavior and conductivity [9,30]. Moreover, by calculating the ratio of the linewidths of the two compounds, a ratio of 0.99 was found. The calculated ratio [44] of the experimentally measured FWHM is basically associated with the selenium crystallographic site occupancy in the matrix of $(\mathrm{PbSe})_5(\mathrm{Bi_2Se_3})_{3m}$. Hence, this finding suggests the presence of an equal number of crystallographic site heterogeneities at the atomic level, as seen by NMR [15,16,19,31,35]. The nearly equal spectrum broadenings that were found are evidence of a structural well ordering of the selenium atoms in the crystal lattice, as well as of a similar amount of possible defects/inhomogeneities in their structure [15,19].

More recently, a comparative crystallographic study by Sassi *et al.* on the same systems suggested that, regardless of *m*, the mean interatomic distances of Se-Pb atoms remain equal, approximately 3.025 Å for $m = 1$ and 3.021 Å for $m = 2$ [13]. By using these interatomic distances, we calculated the dipolar coupling constants to be equal to 0.1734 kHz for $m = 1$ and 0.1741 kHz for $m = 2$, which confirms that the observed line broadening of both compounds cannot be explained by the dipolar broadening and, thus, other contributions play a significant role. Based on the above-mentioned results, we can now argue that both the Knight shift and FWHM of the spectra correlate with the differences in the density of states of the band structures for $(\mathrm{PbSe})_5(\mathrm{Bi_2Se_3})_{3m}$, $m = 1, 2$, and the single and featureless NMR spectra are due to inhomogeneous Knight shifts of the different Se sites (superposition of $^{77}$Se NMR signals) in the lattice [13,43].

To obtain a better understanding of the electronic and structural characteristics of $(\mathrm{PbSe})_5(\mathrm{Bi_2Se_3})_{3m}$, $m = 1, 2$, we also measured the $^{77}$Se nuclear spin-lattice relaxation times ($T_1$) using a saturation recovery method. In nonmagnetic degenerate semiconductors, where the Fermi-contact term is sizable, $T_1$ probes the Fermi surface. In our case, the Fermi-contact term is dominant and any contribution from dipolar or orbital relaxation terms is negligible. Figure 1(b) shows the $^{77}$Se NMR saturation recovery curves of $m = 1$ and 2 at room temperature plotted on a semilogarithmic scale. We used three kinds of fitting methods to evaluate the spin-lattice relaxation time for both materials. This method is commonly used in inhomogeneous materials [31,45,46]. The experimental data were fitted to the single exponential [31,45], the stretched exponential (where $\beta$ is the stretching parameter [45–47], $0 < \beta < 1$), and the double exponential curve [31]. As shown in Fig. 1, the relaxation recovery curves can be characterized well by both the stretched and the double exponential model. This is evidence of an extended distribution of $T_1$ times in both samples caused by the different local environments of Se sites, as well as by the local distortion (and lattice mismatch) due to the layered heterostructure.

We first fit the data using the stretched exponential function, where $\beta$ was found equal to 0.5, independent of temperature. The fit of the experimental data to the stretched exponential curve, shown as solid red line in Fig. 1, gives a spin-lattice relaxation time of $0.41 \pm 0.04$ s for $m = 1$ and $0.24 \pm 0.02$ s for $m = 2$. The obtained $T_1$ value for $m = 2$ is faster than the relaxation value of $m = 1$. However, we note that this model considers a mean $T_1$ value of all different Se sites without distinguishing between the Se sites in PbSe and $Bi_2Se_3$ layers. Hence, we further analyzed our data using a double exponential model. This assumes the presence of two different groups of Se sites that exist in the different layers.

The spin-lattice relaxation rate $(1/T_1)$ governed by carriers (magnetic interaction) in a semiconducting material [36–38,48] can be expressed as

$$\frac{1}{T_1} = \frac{64\pi}{9} n(T) |\Psi(\mathrm{Se})|^4 \gamma_{\mathrm{Se}}^2 \gamma_e^2 \left(\frac{m^3 kT}{2\pi}\right)^{1/2},$$

where $n(T)$ is the carrier density, which is, according to the equation, a temperature-dependent function and related to the relaxation rate $[n(T) \propto (T_1 T^{\frac{1}{2}})]$. $k$ is the Boltzmann constant, $\gamma_{\mathrm{Se}}$ is the gyromagnetic ratio of $^{77}$Se, and $|\Psi(\mathrm{Se})|^2$ represents the conduction electron probability density at a selenium nucleus [10,15]. By using the above equation, we can estimate the difference in the carrier density between the two materials. By calculating the $n_{m=1}^{77}(T)$ and $n_{m=2}^{77}(T)$ at ambient temperature, we obtained that $n_{m=2}^{77}(T)$ is two times higher than $n_{m=1}^{77}(T)$. This calculation reveals a remarkable difference in the $s$-DOS at the Fermi level for these samples. In the recent ARPES study on $m = 1$ and $m = 2$ samples by Nakayama *et al.*, the authors showed a marked difference of the band dispersions near the Fermi level $(E_F)$ in these two samples [4]. This is in agreement with our observations. Particularly, the band structure for $m = 1$ is a single band, whereas for $m = 2$ it consists of multiple bands associated with a shallow dip at the top due to the presence of additional bands that cross $E_F$.

The analysis of the relaxation data with the double exponential function unveiled the presence of two distinct relaxation components across the entire temperature range. We believe that this relaxation model can now represent more appropriately the contributions of the Se groups that are located in the two distinct layers. After extracting the $T_1$ values for both samples, we plotted the relaxation rates divided by temperature $(1/T_1 T)$ as a function of temperature [Figs. 2(a) and 2(b)], since in nonmagnetic semiconductors $1/T_1 T$ provides atomic-level information related to the Fermi surface characteristics [36].

The temperature dependence of the $^{77}$Se $1/T_1 T$ for $m = 1$ ($Pb_5Bi_6Se_{14}$), as shown in Fig. 2, follows a complex $^{77}$Se NMR relaxation mechanism. The first relaxation component of the double exponential recovery function reveals that, initially, $1/T_1 T$ presents a power-law behavior governed by $1/T_1 T \sim T^6$ with increasing temperature. This trend may signal the onset of an energy gap that is quite anisotropic [43]. At high temperatures, $1/T_1 T$ increases with temperature before decreasing from 330 to 420 K. Around 350 K a maximum is achieved. The maximum $1/T_1 T$ value is evidence of an increased charge carrier density dominated by electron carriers. An abrupt decrease of $1/T_1 T$ for $^{77}$Se NMR of $m = 1$ is obtained below 350 K. Since $1/T_1 T$ is dependent on the density of states, the rapid decrease of $1/T_1 T$ is evidence of a (pseudo) gap opening in the density of states [49–51] at the Fermi level of $m = 1$. Furthermore, the $1/T_1 T$ decreases via a power law $(\sim T^6)$. This is a large suppression in $1/T_1 T$ that is rarely found in metallic or semiconducting materials, and which exhibits a temperature-independent $1/T_1 T$ [9,36,39,49–51].

Considering the site-specific sensitivity of NMR relaxivity at the probing nuclear site, such a significant reduction in $1/T_1 T$ clearly suggests a significant change in the density of states [49–51]. The reduction in the DOS indicates the opening of a partially spin-gapped state with residual density of states at the Fermi energy [9,36,37,49–51]. The spin-gap opening begins below 350 K, where the peak temperature of $1/T_1 T$ was developed [Fig. 2(a)]. We may also consider that the observed power-law relaxation trend derives from the distribution of the band dispersions near the Fermi level for $m = 1$, which we found to be not purely parabolic, as previously reported [4]. In addition, the complexity of the crystal structure and/or the existence of structural disorder into the matrix may give rise to further complexities [13].

The temperature dependence of the second relaxation component for the $m = 1$ was found to be stable across the entire experimental temperature range. A temperature-independent $1/T_1 T$ confirms the validity of the Korringa relation [36,37,52], $T_1 T K_s^2 = \frac{\hbar}{4\pi k_B}(\frac{\gamma_e}{\gamma_{\mathrm{Se}}})^2 \approx S$($s$ electrons, Korringa constant) due to the scattering of the conduction electrons near the Fermi surface [36,37]. $S$ is the Korringa constant for $^{77}$Se, which is equal to $7.16 \times 10^{-6}$ s K [53]. Regarding $m = 1$, a small value of $1/T_1 T = 0.005\ \mathrm{s}^{-1}\,\mathrm{K}^{-1}$ was detected. Comparing the observed value of $m = 1$ with the one of a pure Se metal $(1/T_1 T = 0.156\,25\ \mathrm{s}^{-1}\,\mathrm{K}^{-1})$ [54], we can classify $m = 1$ as a semiconducting (narrow-gap semiconductorlike) material. Furthermore, by taking into consideration the nonlinear temperature dependence of the first relaxation component (reduction of DOS at Fermi energy below 350 K, gap opening), we can conclude that the $m = 1$ system is a partially gapped semiconductor with finite DOS at the Fermi level. These $^{77}$Se NMR results agree with Hall mobility data in the same temperature regime [55] reporting a complicated temperature dependence for $m = 1$ around 300 K, as well as a significant electron scattering at the interface between PbSe and $Bi_2Se_3$ layers [13].

The remarkable difference between the band structure of $m = 2$ compared to $m = 1$ is further revealed by NMR in the temperature dependence of $1/T_1 T$ for $m = 2$. As shown in Fig. 2(b), both the short and long relaxation components, as extracted by the double exponential relaxation model,

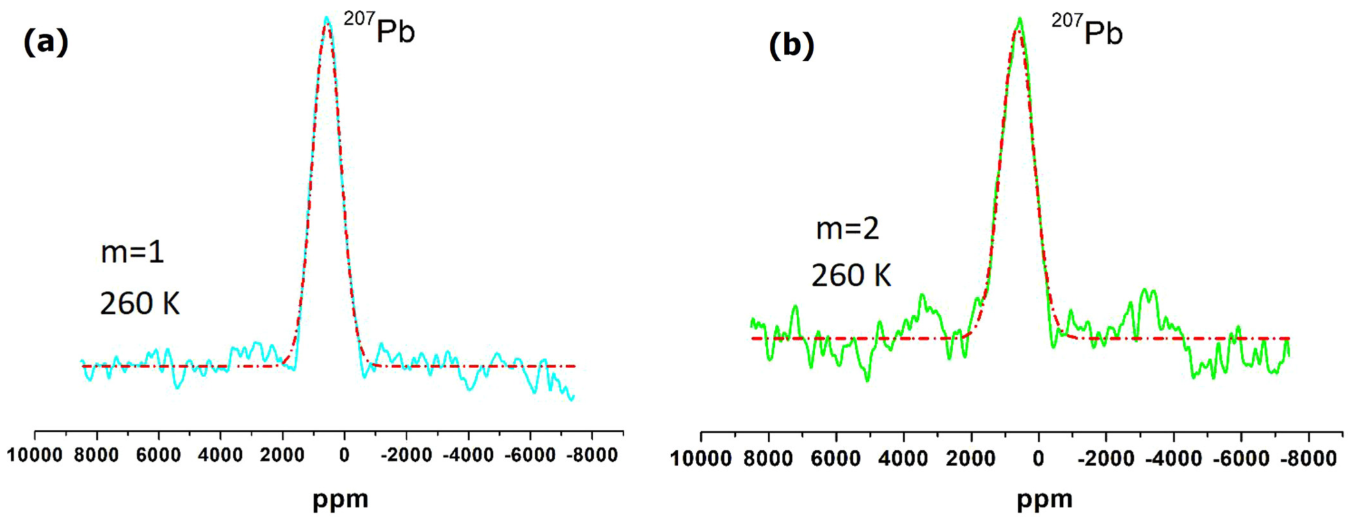

FIG. 3. Solid lines represent $^{207}$Pb NMR spectra obtained from $m = 1$ (a) and $m = 2$ (b) samples of $(\mathrm{PbSe})_5(\mathrm{Bi_2Se_3})_{3m}$ at 260 K. The dashed red lines represent Gaussian fit to the data.

obey the Korringa law [37]. Particularly, in the case of $m = 2$, besides the first relaxation rate component (shown in red) that was found to be almost equal to that of $m = 1$ ($1/T_1T = 0.007\,\mathrm{s^{-1}\,K^{-1}}$), the second component (shown in black) follows again the Korringa relation and not a power-law dependence as was the case for $m = 1$. However, the extracted $1/T_1T$ for the second component of $m = 2$ was 18 times higher ($1/T_1T = 0.126\,\mathrm{s^{-1}\,K^{-1}}$) than its first component. According to the Korringa expression [36,37],

$$\left(\frac{1}{T_1T}\right)_{\text{metal}} = \frac{4\pi k_B}{\hbar}\frac{\gamma_{Se}^2}{{\gamma_e}^2}K^2 \propto [N(E_F)]^2,$$

the $(\frac{1}{T_1T})_{\text{metal}}$ term is proportional to the square of the density of states at the Fermi level, $N(E_F)$ [36,37]. Therefore, the difference in the two obtained $1/T_1T$ values between the two samples indicates that for the $m = 2$ sample the $N(E_F)$ is strongly enhanced relative to $m = 1$. Thus, it agrees with the previously reported differences of the band structures between the two samples [4], which mainly arise due to the enhanced band edge crossing around the Fermi level for $m = 2$ relative to $m = 1$. In addition, our findings are in good agreement with $T$-dependent electrical resistivity studies [13] that reported a metallic behavior (electrical resistivity increases with increasing temperature), which tends to saturate at high temperatures in the case of $m = 2$ ($60\ \mu\Omega\,\mathrm{m}$). By contrast, in the case of $m = 1$ the electrical resistivity is four times higher ($240\ \mu\Omega\,\mathrm{m}$) than that of the $m = 2$ compound and a negative temperature coefficient across the entire temperature range (200–400 K).

Furthermore, the observed temperature dependence of $1/T_1T$ for $m = 2$ rules out the possibility that the material can be described as a gapped semiconductor (similar to $m = 1$), since there is a temperature independence of $1/T_1T$ [Fig. 2(b)]. Hence, the dominance of a conducting-electron-caused relaxation mechanism for the $^{77}$Se nucleus of $m = 2$ across the experimental temperature range is apparent in Fig. 2(b), and aligns with both ARPES [4] and *ab initio* results [8].

More recently, a comparative study by Sassi *et al.* between $m = 1$ and $m = 2$ systems suggested that the difference between the electronic band structure and conductivity of these two systems is caused by the incorporation of the extra $\mathrm{Bi_2Se_3}$ layer into the matrix [13,55]. The additional $\mathrm{Bi_2Se_3}$ layer sufficiently modifies the electronic band structure by increasing $N(E_F)$, which is in line with the present difference in the NMR spin-lattice relaxation and Knight shift results between $m = 1$ and $m = 2$. Consequently, crystal structure plays a less pivotal role in the band structure and electrical characteristics of the $(\mathrm{PbSe})_5(\mathrm{Bi_2Se_3})_{3m}$ heterostructure than the actual number of $\mathrm{Bi_2Se_3}$ and PbSe layers. Moreover, as Segawa *et al.* [43] suggested for the same materials, the presence of the PbSe layer in the matrix acts as a block layer for the charge transport of the whole system.

The $^{207}$Pb NMR spectral ($^{207}K$, FWHM) characteristics and the $^{207}$Pb nuclear spin-lattice relaxation data of both systems were further examined as a function of temperature. Figure 3 demonstrates the $^{207}$Pb NMR spectra acquired at 260 K from both materials. Both spectra are Gaussian with frequency shifts at 581 ppm ($m = 1$) and 638 ppm ($m = 2$), whereas the line broadening is well described by a FWHM of 1058 ppm ($m = 1$) and 1122 ppm ($m = 2$) at 260 K. Figure 4 shows the temperature variation of the $^{207}$Pb Knight shift ($^{207}K$) for $m = 1$ and $m = 2$ samples. The measured value of $^{207}K$ for all samples has a positive sign and is nearly independent of temperature below room temperature. However, in Fig. 4 the temperature dependence of $^{207}K$ reveals a marked difference between $m = 1$ and $m = 2$. Particularly, in the low-temperature regime ($T < 330\,\mathrm{K}$), $^{207}K$ takes a constant value of approximately 606 ppm for $m = 1$ and 645 ppm for $m = 2$.

Upon warming above 350 K, the NMR lineshift of $m = 2$ becomes temperature dependent and gradually adopts a power-law dependency ($\propto T^{3/2}$). A change in the NMR lineshift above 350 K corresponds to the case of a gapless semiconductor (or semimetal) mechanism [17,56], as shown in the inset of Fig. 4. For $m = 2$, the aforementioned mechanism seems to be justified by the existence of six

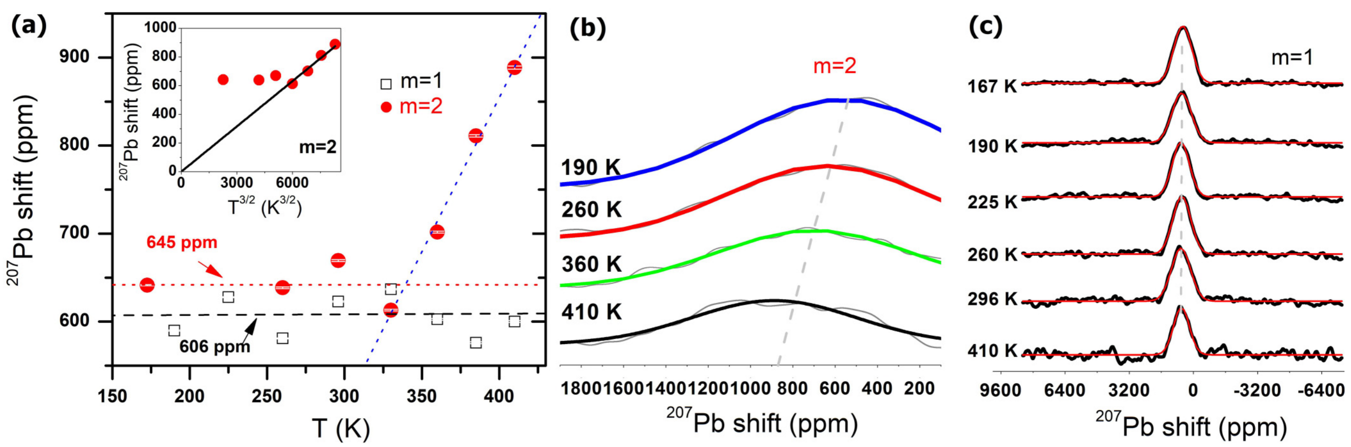

FIG. 4. (a) Temperature dependence of the $^{207}$Pb Knight shifts of $(\mathrm{PbSe})_5(\mathrm{Bi_2Se_3})_{3m,m=1,2}$, where the $m = 1$ is shown as black open squares and $m = 2$ as red spheres. The inset shows the power-law temperature dependence of the $^{207}$Pb shift for the $m = 2$ case (red spheres). The remaining two graphs depict the temperature dependence of the $^{207}$Pb lineshape for $m = 2$ (b) and $m = 1$ (c).

dispersive features that cross the Fermi surface between two time-reversal-invariant momenta ($\bar{\Gamma}$, $\bar{M}$), as also shown in ARPES studies [4]. A similar exponent value has recently been observed in topologically nontrivial half-Heusler materials due to the orbital diamagnetism induced by enhanced spin-orbit interactions [17,56]. Contrary to $m = 2$, the $^{207}K$ of $m = 1$ remains constant across the entire experimental temperature range, as expected for semiconducting materials (Fig. 4). We argue that such a striking difference in $^{207}K$ between $m = 1$ and $m = 2$ originates from the difference in the topology of the band dispersions near the Fermi level that is strongly modified by the addition of a $\mathrm{Bi_2Se_3}$ ($m = \infty$) layer into the matrix, as we have previously detected by $^{77}$Se NMR.

More detailed information can be extracted from the analysis of the $^{207}$Pb spin-lattice relaxation ($1/T_1$) data. The results of the $^{207}$Pb saturation recovery measurements at ambient temperature are shown in Fig. 5. The data for both materials are well fitted by a stretched exponential function [45–47], where the stretching parameter ($\beta$) is presented by the solid line in Fig. 5 (inset). The adequateness of the stretched exponential function is based on the numerous crystallographically inequivalent Pb sites in the matrix caused by lattice distortion and lattice mismatch along the different layers, regardless of $m$. The stretching factor takes into account the broad distribution of $T_1$ over the Pb sites in the samples, and was found temperature independent and equal to $\beta = 0.65$ for both materials.

The temperature dependence of $^{207}$Pb $1/T_1$ for both materials is reported in Fig. 6. In particular, Fig. 6 presents semilogarithmic plots of $T_1$ versus reciprocal temperature ($1/T$), where the red solid lines represent the thermally activated mechanism [15,48,57], where the linear least-squares fit provides the activation energies of the relaxation processes for $m = 1$ and $m = 2$, equal to E = 56.9 meV (or 660 K) for $m = 1$ and 75.7 meV (or 878 K) for $m = 2$, respectively.

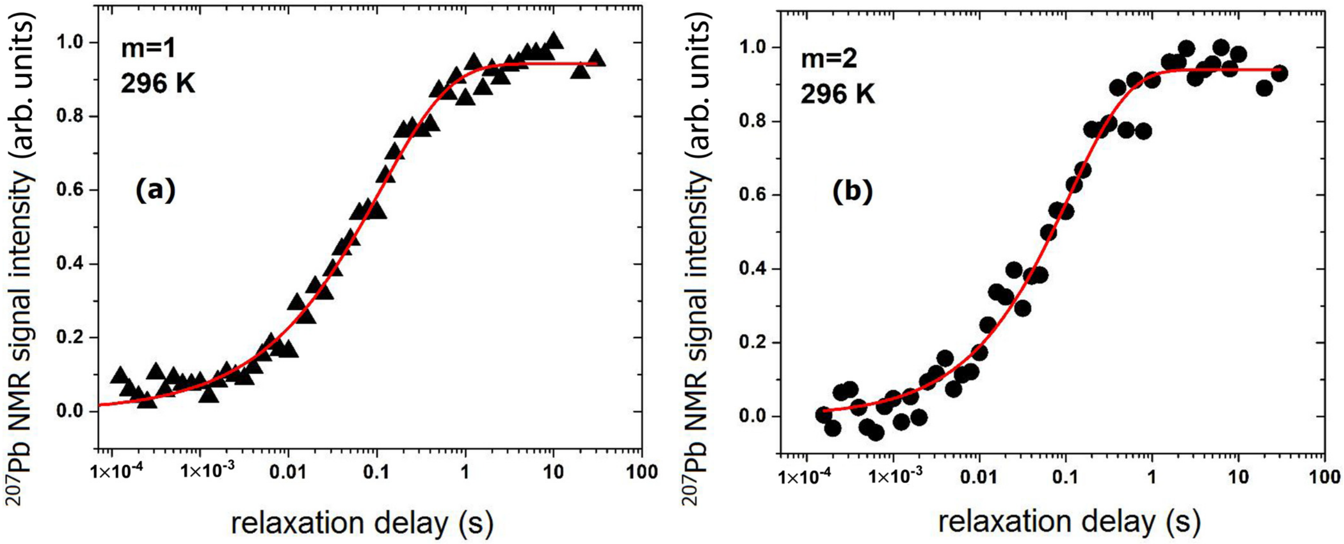

FIG. 5. $^{207}$Pb NMR saturation recovery data for $m = 1$ (a) and $m = 2$ (b) of $(\mathrm{PbSe})_5(\mathrm{Bi_2Se_3})_{3m}$ at ambient temperature. The solid red line represents the fit of a stretched exponential model to the recovery data, as described in the text.

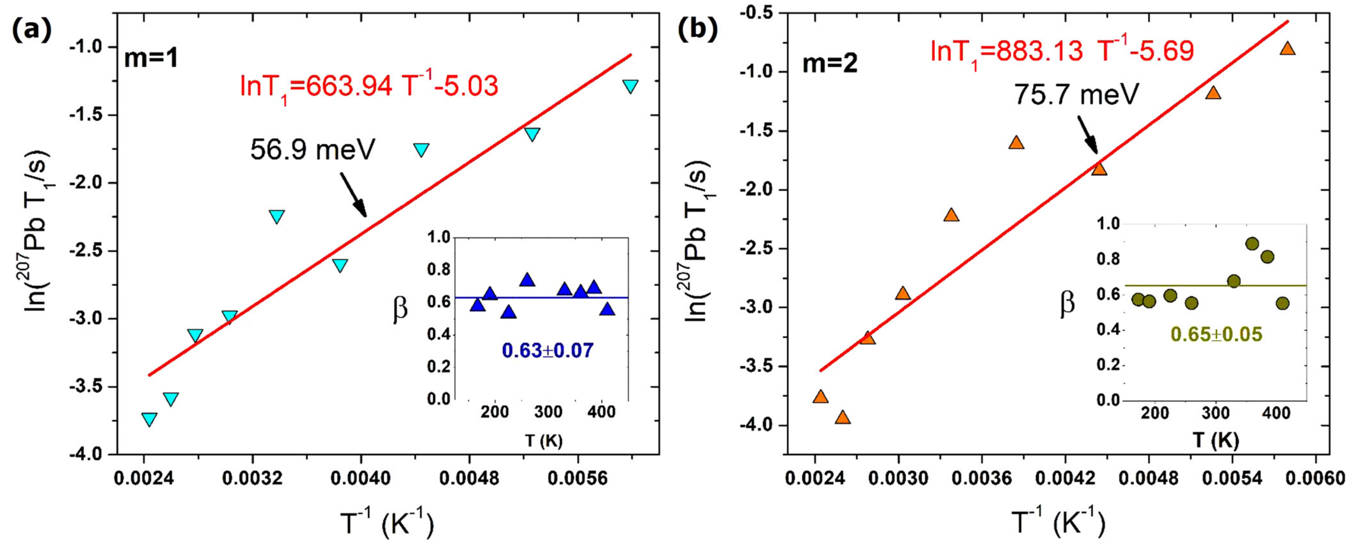

FIG. 6. Semilogarithmic plot of the $^{207}$Pb nuclear spin-lattice relaxation data versus reciprocal temperature for $m = 1$ (a) and $m = 2$ (b) of $(\mathrm{PbSe})_5(\mathrm{Bi_2Se_3})_{3m}$. The solid red line represents a thermal activation mechanism caused by thermally generated mobile carriers, as described in the text. The stretching factors ($\beta$) for both materials as a function of temperature are shown in the insets.

The magnitude of the extracted $E$ for $m = 2$ is about 1.3 times higher than that for $m = 1$ (Fig. 6). The absence of the Korringa law, as opposed to the $^{77}$Se NMR results for $m = 2$, implies a striking difference in the way that each nucleus ($^{77}$Se or $^{207}$Pb) *"feels"* the change in the topology of the band structure during the band inversion. Since the spin susceptibility of the electrons around each different nucleus site (Se and Pb) affects differently the hyperfine field couplings for each nucleus, the $1/T_1$ and Knight shift parameters are not expected to exhibit similar behavior. This site-selective sensitivity of the NMR parameters is an advantage compared to the volume-averaged techniques (e.g., transport, specific heat measurements) [6,9,30,35].

In Fig. 6, the higher activation energy detected from $^{207}$Pb NMR in Pb sites of $m = 2$ coincides with recent band structure calculations [8] of the $m = 2$ system, which have shown that Pb bands lie below the Fermi energy and are partially filled with holes around Γ, while there is a gap of approximately 20 meV at the bottom of the Dirac-cone dispersion. Besides the presence of an additional hybridization gap (20 meV) [8,4] around the Fermi level at Γ for $m = 2$, charge-density calculations reported that the electrons of Pb atoms are transferred to interstitial regions of the lattice leaving the Pb sites electronically deprived, which is in line with the nonappearance of the Korringa mechanism (i.e., metallicity) in the present $^{207}$Pb NMR results (contrary to the $^{77}$Se NMR results in $m = 2$). Furthermore, the shorter $T_1$ obtained for $m = 1$ in comparison to $m = 2$ is very strong proof of the higher carrier density surrounding the Pb sites in $m = 1$. This can be explained by the swiftness of the spin-lattice relaxation process that is directly related to the number of electrons engaged in the magnetic relaxation channel. Our results, however, do not rule out the possibility that localized defect states may be present in the bandgap region of both $m = 1$ and $m = 2$. In specific, we found that the extracted activation energies obtained for both compounds match also well the activation energy of 69.2 meV obtained from the $^{207}$Pb NMR data in PbSe at the high-temperature regime ($T > 250$ K) [15]. The larger activation energy detected for $m = 2$ was equal to 75.7 meV and, compared to $m = 1$, is closer to the 87 meV activation energy that has been detected via NMR in the high-temperature regime of other topological insulating materials, such as $\mathrm{Bi_2Te_3}$ [18,19]. Additionally, previous studies on PbSe referred to the presence of localized states varying from 50 to 70 meV in the band gap [15,58,59], which is very close to the obtained values in the present study. Hence, the impact of localized defect states in the narrow bandgap region (interband excitations) should be also considered for the interpretation of the topological insulating properties of the $(\mathrm{PbSe})_5(\mathrm{Bi_2Se_3})_{3m}$ family. It would be interesting to investigate the relaxation characteristics of the $m > 2$ series, as previous studies have reported that both $m = 3$ and $m = 4$ exhibit similar transport properties despite the additional $\mathrm{Bi_2Se_3}$ layers. Furthermore, the adverse impact of the presence of different types of carriers and native defects on the electronic and thermoelectric characteristics of alloyed ternary and quaternary TIs has been previously demonstrated via NMR and Seebeck coefficient studies [9].

## IV. CONCLUSIONS

In conclusion, we investigated the recently discovered topologically nontrivial features at the density of states in the vicinity of the Fermi level of $\mathrm{Pb_5Bi_6Se_{14}}$ ($m = 1$) and $\mathrm{Pb_5Bi_{12}Se_{23}}$ ($m = 2$) with $^{77}$Se and $^{207}$Pb NMR as a function of temperature. Combining the Seebeck coefficient values with the sign and magnitude of the $^{77}$Se NMR shifts, the $n$-type character of these compounds was revealed. In the case of $\mathrm{Pb_5Bi_6Se_{14}}$, the $^{207}$Pb NMR shifts were found to be temperature independent, while the $^{207}$Pb shift for $\mathrm{Pb_5Bi_{12}Se_{23}}$ revealed a remarkable enhancement above 350 K following a power-law temperature dependence ($\propto T^{3/2}$), as opposed to the simple semiconducting behavior observed in $\mathrm{Pb_5Bi_6Se_{14}}$. Conversely, the $^{77}$Se nuclear spin-lattice relaxation rate divided by temperature ($1/T_1T$) yielded a peak around 350 K and then decreased as $1/T_1T \sim T^6$, followed by an almost constant product $1/T_1T$ in the high-temperature regime, whereas the second part remained temperature independent. The $^{77}$Se NMR relaxation data in $\text{Pb}_5\text{Bi}_{12}\text{Se}_{23}$ for both components are well described by free-electron behavior (Korringa law) across the entire temperature range, a signature of the metalliclike properties of this system. Even though the band structure between these two materials differs substantially, the $^{207}$Pb NMR relaxation results for both materials follow a thermally activated relaxation pathway, in agreement with the presence of a hybridization gap in the topological states for $m = 2$ and the presence of localized defect states in the band gap of PbSe [15,58,59] as well as an inhomogeneous distribution of a high defect content in $\text{Bi}_2\text{Se}_3$ [31]. Yet, as seen in Fig. 6, the resultant activation gaps differ remarkably, being approximately 56.5 meV ($m = 1$) and 75.7 meV ($m = 2$), because of the different defect level and charge density at the Pb sites of each compound. The present study clarifies the nature of the heterostructure $(\text{PbSe})_5(\text{Bi}_2\text{Se}_3)_{3m}$ family and the effect of its layers on physical properties. This knowledge is relevant for the design of future, heterostructure-based topological materials.

## ACKNOWLEDGMENTS

Work at Argonne (sample preparation, characterization, and crystal growth) is supported by the US DOE, Office of Basic Energy Science, Materials Science and Engineering Division. This research was supported by the Defense Advanced Research Project Agency (DARPA), Award No. N66001-12-1-4034. We acknowledge the use of instruments at the Molecular Instrumentation (MIC) facility at UCLA.

---

[1] M. G. Kanatzidis, Structural evolution and phase homologies for “design” and prediction of solid-state compounds, Acc. Chem. Res. **38**, 359 (2005).

[2] A. Politano, L. Viti, and M. S. Vitiello, Optoelectronic devices, plasmonics, and photonics with topological insulators, APL Mater. **5**, 035504 (2017).

[3] L. Fang, C. C. Stoumpos, Y. Jia, A. Glatz, D. Y. Chung, H. Claus, U. Welp, W.-K. Kwok, and M. G. Kanatzidis, Dirac fermions and superconductivity in the homologous structures $(\text{Ag}_x\text{Pb}_{1-x}\text{Se})_5(\text{Bi}_2\text{Se}_3)_{3m}$ ($m = 1, 2$), Phys. Rev. B **90**, 020504(R) (2014).

[4] K. Nakayama, K. Eto, Y. Tanaka, T. Sato, S. Souma, T. Takahashi, K. Segawa, and Y. Ando, Manipulation of Topological States and the Bulk Band Gap Using Natural Heterostructures of a Topological Insulator, Phys. Rev. Lett. **109**, 236804 (2012).

[5] Z. Zhu, Y. Cheng, and U. Schwingenschlögl, Band inversion mechanism in topological insulators: A guideline for materials design, Phys. Rev. B **85**, 235401 (2012).

[6] D. Koumoulis, T. C. Chasapis, B. Leung, R. E. Taylor, C. C. Stoumpos, N. P. Calta, M. G. Kanatzidis, and L.-S. Bouchard, Site-specific contributions to the band inversion in a topological crystalline insulator, Adv. Electron. Mater. **1**, 1500117 (2015).

[7] J. O. Dimmock, I. Melngailis, and A. J. Strauss, Band Structure and Laser Action in $\text{Pb}_x\text{Sn}_{1-x}\text{Te}$, Phys. Rev. Lett. **16**, 1193 (1966).

[8] H. Momida, G. Bihlmayer, S. Blugel, K. Segawa, Y. Ando, and T. Oguchi, Topological interface states in the natural heterostructure $(\text{PbSe})_5(\text{Bi}_2\text{Se}_3)_6$ with BiPb defects, Phys. Rev. B **97**, 035113 (2018).

[9] T. C. Chasapis, D. Koumoulis, B. Leung, N. P. Calta, S.-H. Lo, V. P. Dravid, L.-S. Bouchard, and M. G. Kanatzidis, Two-band model interpretation of the *p*- to *n*- transition in ternary tetradymite topological insulators, APL Mater. **3**, 083601 (2015).

[10] X. Zhang, Z. Hou, Y. Wang, G. Xu, C. Shi, E. Liu, X. Xi, W. Wang, G. Wu, and X. Zhang, NMR evidence for the topologically nontrivial nature in a family of half-Heusler compounds, Sci. Rep. **6**, 23172 (2016).

[11] B. Nowak and D. Kaczorowski, NMR as a probe of band inversion in topologically nontrivial half-Heusler compounds, J. Phys. Chem. C **118**, 18021 (2014).

[12] M. Ohta, D. Y. Chung, M. Kunii, and M. G. Kanatzidis, Low lattice thermal conductivity in $\text{Pb}_5\text{Bi}_6\text{Se}_{14}$, $\text{Pb}_3\text{Bi}_2\text{S}_6$, and $\text{PbBi}_2\text{S}_4$: Promising thermoelectric materials in the cannizzarite, lillianite, and galenobismuthite homologous series, J. Mater. Chem. A **2**, 20048 (2014).

[13] S. Sassi, C. Candolfi, G. Delaizir, S. Migot, J. Ghanbaja, C. Gendarme, A. Dauscher, B. Malaman, and B. Lenoir, Crystal structure and transport properties of the homologous compounds $(\text{PbSe})_5(\text{Bi}_2\text{Se}_3)_{3m}$ ($m = 2$, 3), Inorg. Chem. **57**, 422 (2018).

[14] R. K. Harris and B. E. Mann, *NMR and the Periodic Table* (Academic Press, London, 1998).

[15] D. Koumoulis, R. E. Taylor, D. King, and L.-S. Bouchard, NMR study of native defects in PbSe, Phys. Rev. B **90**, 125201 (2014).

[16] R. E. Taylor, F. Alkan, D. Koumoulis, M. P. Lake, D. King, C. Dybowski, and L.-S. Bouchard, A combined NMR and DFT study of narrow gap semiconductors: The case of PbTe, J. Phys. Chem. C **117**, 8959 (2013).

[17] C. Shi, X. Xi, Z. Hou, X. Zhang, G. Xu, E. Liu, W. Wang, W. Wang, J. Chen, and G. Wu, NMR investigation of atomic and electronic structures of half-Heusler topologically nontrivial semimetals, Phys. Status Solidi B **252**, 357 (2014).

[18] D. Koumoulis, T. C. Chasapis, R. E. Taylor, M. P. Lake, D. King, N. N. Jarenwattananon, G. A. Fiete, M. G. Kanatzidis, and L.-S. Bouchard, NMR Probe of Metallic States in Nanoscale Topological Insulators, Phys. Rev. Lett. **110**, 026602 (2013).

[19] D. Koumoulis, B. Leung, T. C. Chasapis, R. E. Taylor, D. King, M. G. Kanatzidis, and L.-S. Bouchard, Understanding bulk defects in topological insulators from nuclear-spin interactions, Adv. Funct. Mater. **24**, 1519 (2014).

[20] R. Guehne, V. Chlan, G. V. M. Williams, S. V. Chong, K. Kadowaki, A. Pöppl, and J. Haase, Unusual $^{209}$Bi NMR quadrupole effects in topological insulator $\text{Bi}_2\text{Se}_3$, J. Magn. Res. **302**, 34 (2019).

[21] B.-L. Young, Z.-Y. Lai, Z. Xu, A. Yang, G. D. Gu, Z.-H. Pan, T. Valla, G. J. Shu, R. Sankar, and F. C. Chou, Probing the bulk electronic states of $Bi_2Se_3$ using nuclear magnetic resonance, Phys. Rev. B **86**, 075137 (2012).

[22] D. Koumoulis, R. E. Taylor, J. McCormick, Y. N. Ertas, L. Pan, X. Che, K. L. Wang, and L.-S. Bouchard, Effects of Cd vacancies and unconventional spin dynamics in the Dirac semimetal $Cd_3As_2$, J. Chem. Phys. **147**, 084706 (2017).

[23] D. Koumoulis, G. D. Morris, L. He, X. Kou, D. King, D. Wang, M. D. Hossain, K. L. Wang, G. A. Fiete, M. G. Kanatzidis, and L.-S. Bouchard, Nanoscale $\beta$-nuclear magnetic resonance depth imaging of topological insulators, Proc. Natl. Acad. Sci. USA **112**, E3645 (2015).

[24] D. Koumoulis, J. P. Scheifers, R. Touzani, B. P. T. Fokwa, and L.-S. Bouchard, Direct chemical fine-tuning of electronic properties in $Sc_2Ir_{6-x}Pd_xB$, ChemPhysChem. **17**, 2972 (2016).

[25] D. M. Nisson and N. J. Curro, Nuclear magnetic resonance Knight shifts in the presence of strong spin–orbit and crystal-field potentials, New J. Phys. **18**, 073041 (2016).

[26] W. A. MacFarlane, C. B. L. Tschense, T. Buck, K. H. Chow, D. L. Cortie, A. N. Hariwal, R. F. Kiefl, D. Koumoulis, C. D. P. Levy, I. McKenzie, F. H. McGee, G. D. Morris, M. R. Pearson, Q. Song, D. Wang, Y. S. Hor, and R. J. Cava, $\beta$-detected NMR of $^8Li^+$ in Bi, Sb, and the topological insulator $Bi_{0.9}Sb_{0.1}$, Phys. Rev. B **90**, 214422 (2014).

[27] S. Boutin, J. Ramírez-Ruiz, and I. Garate, Tight-binding theory of NMR shifts in topological insulators $Bi_2Se_3$ and $Bi_2Te_3$, Phys. Rev. B **94**, 115204 (2016).

[28] D. M. Nisson, A. P. Dioguardi, P. Klavins, C. H. Lin, K. Shirer, A. C. Shockley, J. Crocker, and N. J. Curro, Nuclear magnetic resonance as a probe of electronic states of $Bi_2Se_3$, Phys. Rev. B **87**, 195202 (2013).

[29] S. Mukhopadhyay, S. Kramer, H. Mayaffre, H. F. Legg, M. Orlita, C. Berthier, M. Horvatic, G. Martinez, M. Potemski, B. A. Piot, A. Materna, G. Strzelecka, and A. Hruban, Hyperfine coupling and spin polarization in the bulk of the topological insulator $Bi_2Se_3$, Phys. Rev. B **91**, 081105 (2015).

[30] E. M. Levin, T. M. Riedemann, A. Howard, N. H. Jo, S. L. Bud'ko, P. C. Canfield, and T. A. Lograsso, $^{125}$Te NMR and Seebeck effect in $Bi_2Te_3$ synthesized from stoichiometric and Te-rich melts, J. Phys. Chem. C **120**, 25196 (2016).

[31] R. E. Taylor, B. Leung, M. Lake, and L.-S. Bouchard, Spin–lattice relaxation in bismuth chalcogenides, J. Phys. Chem. C **116**, 17300 (2012).

[32] N. M. Georgieva, D. Rybicki, R. Guehne, G. V. M. Williams, S. V. Chong, K. Kadowaki, I. Garate, and J. Haase, $^{77}$Se nuclear magnetic resonance of topological insulator $Bi_2Se_3$, J. Phys. Rev. B **93**, 195120 (2016).

[33] K. Matano, M. Kriener, K. Segawa, Y. Ando, and G. Zheng, Spin-rotation symmetry breaking in the superconducting state of $Cu_xBi_2Se_3$, Nat. Phys. **12**, 852 (2016).

[34] J. K. Park, C. Y. Lee, and C. Kim, NMR probe of bulk electronic structures in $H^+$ beam irradiated $Bi_2Te_3$ topological insulator, Curr. Appl. Phys. **19**, 291 (2019).

[35] E. M. Levin, J. P. Heremans, M. G. Kanatzidis, and K. Schmidt-Rohr, Electronic inhomogeneity in *n*- and *p*-type PbTe detected by $^{125}$Te NMR, Phys. Rev. B **88**, 115211 (2013).

[36] D. Wolf, *Spin-Temperature and Nuclear-Spin Relaxation in Matter* (Clarendon Press, Oxford, 1979).

[37] J. Korringa, Nuclear magnetic relaxation and resonance lineshift in metals, Physica (Amsterdam) **16**, 601 (1950).

[38] C. S. Lue, B. X. Xie, and C. P. Fang, NMR evidence for the coexistence of double structure in CaAlSi, Phys. Rev. B **74**, 014505 (2006).

[39] M. N. Alexander, P. L. Sagalyn, S. D. Senturia, and C. R. Hewes, Nuclear spin relaxation study of the electronic structure of lead telluride, J. Nonmet **1**, 251 (1973).

[40] M. J. Hirsch and D. F. Holcomb, NMR Study of Si:As and Si:P near the metal-insulator transition, Phys. Rev. B **33**, 2520 (1986).

[41] A. O. Antonenko, D. Y. Nefedov, E. V. Charnaya, S. V. Naumov, and V. V. Marchenkov, $^{77}$Se low-temperature NMR in the $Bi_2Se_3$ single crystalline topological insulator, Appl. Magn. Reson. **49**, 599 (2018).

[42] C. C. Yuan, J. F. Xiang, X. Xi, and W. H. Wang, NMR Signature of Evolution of Ductile-to-Brittle Transition in Bulk Metallic Glasses, Phys. Rev. Lett. **107**, 236403 (2011).

[43] K. Segawa, A. A. Taskin, and Y. Ando, PbBiSe: A new member of the homologous series forming topological insulator heterostructures, J. Solid State Chem. **221**, 196 (2015).

[44] The area under an NMR spectrum is proportional to the number of nuclei that resonate within the corresponding frequency window. However, the NMR linewidth not only reflects the distribution of local chemical environments, but is also sensitive to the distribution of native defects, particularly in the cases of $Bi_2Se_3$ and PbSe, as already reported in Refs. [15,19]. By assuming that $m = 1$ and $m = 2$ have the same defect density, the ratio of the FWHM will be an indication of the site occupancy between these materials. Two recent studies (see Refs. [30,34]) have shown that as the defect/vacancy density increases the linewidth also increases (causing an asymmetric line shape in these TI materials). These studies have shown that defect and/or vacancy regions segregate into domains in both materials. The FWHM of a spectrum represents not only the different selenium sites, but rather mainly the inhomogeneous distribution of the defects with the increased charge carrier concentrations possessing different Knight shifts.

[45] R. Taylor, P. A. Beckmann, S. Bai, and C. Dybowski, $^{127}$I and $^{207}$Pb solid-state NMR spectroscopy and nuclear spin relaxation in $PbI_2$: A preliminary study, J. Phys. Chem. C **118**, 9143 (2014).

[46] D. C. Johnston, Stretched exponential relaxation arising from a continuous sum of exponential decays, Phys. Rev. B **74**, 184430 (2006).

[47] D. Bono, J. Hartig, M. Huber, H. Schnöckel, and L. J. de Jongh, $^{27}$Al NMR study of the metal cluster compound $Al_{50}C_{120}H_{180}$, J. Cluster Sci. **18**, 319 (2007).

[48] M. Shroyer, W. W. Warren, and A. I. Ryskin, Nuclear spin-lattice relaxation by optically bistable defects in $CdF_2$:In, Phys. Rev. B **65**, 165202 (2002).

[49] C. S. Lue, S. H. Yang, T. H. Su, and B.-L. Young, NMR evidence for the partially gapped state in $CeOs_2Al_{10}$, Phys. Rev. B **82**, 195129 (2010).

[50] K. Kang, M. Lee, N. H. Sung, and B. K. Cho, Pseudogap opening in single-crystal $YMn_4Al_8$ investigated through $^{55}$Mn and $^{27}$Al NMR measurements, Phys. Rev. B **98**, 224412 (2018).

[51] C.-S. Lue and J. H. Ross, Pseudogap in $Fe_2VGa$: NMR evidence, Phys. Rev. B **63**, 054420 (2001).

[52] P. Babu, A. Lewera, J. H. Chung, R. Hunger, W. Jaegermann, N. Alonso-Vante, A. Wieckowski, and E. Oldfield, Selenium becomes metallic in Ru−Se fuel cell catalysts: An EC-NMR and XPS investigation, J. Am. Chem. Soc. **129**, 15140 (2007).

[53] B. S. Zelakiewicz, T. Yonezawa, and Y. Tong, Observation of selenium-77 nuclear magnetic resonance in octaneselenol-protected gold nanoparticles, J. Am. Chem. Soc. **126**, 8112 (2004).

[54] L. L. Lumata, K. Y. Choi, J. S. Brooks, A. P. Reyes, P. L. Kuhns, G. Wu, and X. H. Chen, $^{77}$Se and $^{63}$Cu NMR studies of the electronic correlations in $\mathrm{Cu}_x\mathrm{TiSe}_2$ ($x = 0.05$, 0.07), J. Phys.: Condens. Matter **22**, 295601 (2010).

[55] S. Sassi, C. Candolfi, V. Ohorodniichuk, C. Gendarme, P. Masschelein, A. Dauscher, and B. Lenoir, Thermoelectric properties of polycrystalline $n$-type $\mathrm{Pb}_5\mathrm{Bi}_6\mathrm{Se}_{14}$, J. Electron. Mater. **46**, 5 (2017).

[56] I. M. Tsidilkovski, *Electron Spectrum of Gapless Semiconductors*, Springer Series in Solid-State Sciences Vol. 116 (Springer, New York, 1996).

[57] G. Neue, S. Bai, R. E. Taylor, P. A. Beckmann, A. J. Vega, and C. Dybowski, $^{119}$Sn spin-lattice relaxation in $\alpha$-$\mathrm{SnF}_2$, Phys. Rev. B **79**, 214302 (2009).

[58] M. F. Kotkata, M. S. Al-Kotb, and I. G. El-Houssieny, Observation of the Meyer-Neldel rule in nanocrystalline PbSe thin films, Phys. Scr. **89**, 115805 (2014).

[59] W.-F. Li, C.-M. Fang, M. Dijkstra, and M. A. van Huis, The role of point defects in PbS, PbSe and PbTe: A first principles study, J. Phys.: Condens. Matter **27**, 355801 (2015).